International Geology Review
Publication details, including instructions for authors and subscription information:
http://www.tandfonline.com/loi/tigr20

The deep water cycle and flood basalt volcanism

Alexei V. Ivanov [a] & Konstantin D. Litasov [b]

[a] Institute of the Earth's Crust, Siberian Branch, Russian Academy of Sciences , Lermontov street 128, 664033 , Irkutsk , Russia

[b] Institute of Geology and Mineralogy, Siberian Branch, Russian Academy of Sciences , Novosibirsk , Russia

Published online: 30 Jul 2013.

To cite this article: International Geology Review (2013): The deep water cycle and flood basalt volcanism, International Geology Review

To link to this article: http://dx.doi.org/10.1080/00206814.2013.817567

International Geology Review, 2013
http://dx.doi.org/10.1080/00206814.2013.817567

Taylor & Francis
Taylor & Francis Group

The deep water cycle and flood basalt volcanism

Alexei V. Ivanov[a]* and Konstantin D. Litasov[b]

[a]*Institute of the Earth's Crust, Siberian Branch, Russian Academy of Sciences, Lermontov street 128, 664033 Irkutsk, Russia;* [b]*Institute of Geology and Mineralogy, Siberian Branch, Russian Academy of Sciences, Novosibirsk, Russia*

(*Accepted 17 June 2013*)

Experimental data combined with numerical simulations suggest that fast-subducting oceanic slabs are cold enough to carry a significant amount of H_2O into the deep mantle in antigorite; with increasing depth, this mineral undergoes solid–solid transitions to phase A and then to phase E and/or wadsleyite. Ice VII and clathrate hydrates can also be stable under pressure and temperature (PT) conditions of cold slabs and represent other potential phases for water transport into the deep mantle. Cold slabs are expected to stagnate in the mantle transition zone. With time, they are heated to the temperature of the ambient transition zone and release excess water as a H_2O-bearing fluid. This may cause voluminous melting of overlying upper mantle rocks. If such a process operates in nature, magmas geochemically similar to island-arc basalts are expected to appear in places relatively remote from active arcs at the time of their emplacement. Dolerites of the southeastern margin of the Siberian flood basalt province, located about 700 km from suggested trench, were probably associated with the fast (cold) subduction of the Mongolia–Okhotsk oceanic slab, and originated by the dehydration of the stagnant slab in the transition zone. We show that the influence of the subduction-related deep water cycle on Siberian flood basalt magmatism gradually diminished with increasing distance from the subduction zone. Thus, the unique size and volume of the Siberian flood basalt province could have originated due to long-term underflow beneath Siberia with or without the existence of a lower mantle plume.

Keywords: flood basalts; stagnant slab; transition zone; deep water cycle; mantle plumes

Introduction

Subducting slabs can transport significant amounts of water into the deep Earth (Peacock 1990). Major hydrated parts of the slab are oceanic sediments and underlying basaltic crust. Experimental studies of simplified and natural H_2O-bearing systems show that subducted oceanic sediments may contain high-pressure topaz-OH + phase Egg, and basaltic crust can transport water as zoicite, lawsonite, and amphibole (e.g. Williams and Hemley 2001; Arcay *et al*. 2007). Significant hydration of the uppermost peridotite layer of the slab has also been argued (e.g. Williams and Hemley 2001; Komabayashi 2006; Arcay *et al*. 2007; Ivandic *et al*. 2010). Hydrated peridotite can transport water into the deep mantle in antigorite (serpentine), which transforms with depth to dense-hydrous-magnesium-silicates by solid–solid transformations (e.g. Litasov and Ohtani 2003; Komabayashi *et al*. 2005). In the mantle transition zone, the major H_2O-bearing phases are wadsleyite and ringwoodite (e.g. Ohtani and Litasov 2006; Litasov and Ohtani 2007). Numerical calculations of possible pressure and temperature (PT) paths of cold subducting slabs suggest that water can be also subducted as high-pressure ice VII (Bina and Navrotsky 2000).

Despite the wide interest in hydrogen-bearing mineral stability fields within the slabs and deep mantle and conditions of melting in hydrated deep mantle (e.g. Williams and Hemley 2001; Ohtani 2005; Sakamaki *et al*. 2006), few studies have been published on the geochemical significance of the deep water cycle (e.g. Bercovici and Karato 2003; Ivanov and Balyshev 2005). Bercovici and Karato (2003) forwarded a hypothesis of a transition zone water filter, in which slabs dehydrate in the mantle transition zone on their passage into the lower mantle (Figure 1). According to this idea, H_2O-bearing fluid enriched in incompatible elements is stored in the transition zone and later influences the trace-element budget of mantle plumes on their ascent from the lower mantle. This hypothesis was designed to explain the difference in trace element and radiogenic isotope geochemistry between ocean island basalts and mid-ocean ridge basalts. Ivanov and Balyshev (2005) and Komabayashi (2006) independently forwarded a hypothesis in which dehydration of stagnant oceanic slabs

*Corresponding author. Email: aivanov@crust.irk.ru

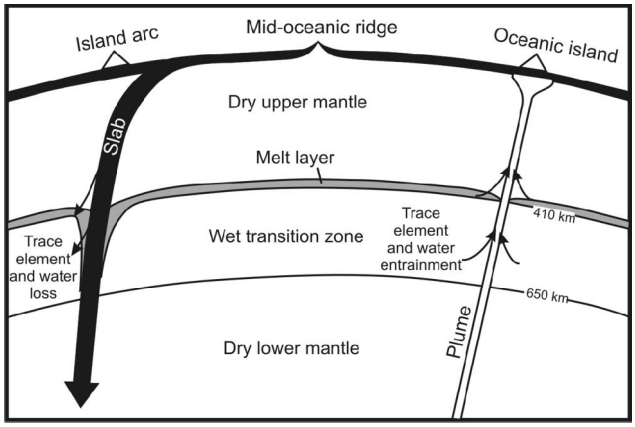

Figure 1. Model of the transition mantle water filter (modified after Bercovici and Karato 2003).

in the transition zone may cause igneous activity similar to island-arc magmatism (Figure 2). This hypothesis is suitable for interpreting volcanism in some back-arc and even intra-continental tectonic settings. In this paper, we test the latter hypothesis with an example of Siberian flood basalts, which formed in a back-arc tectonic setting of the Mongolia–Okhotsk subduction system. Before considering the Siberian flood basalts, we start with a brief review of evidence for the deep water cycle via the fast slab subduction and the slab stagnation in the transition zone.

Experimental data on deep water cycle

Figure 3 summarizes the stability of hydrous minerals from experiments in the $CaO–MgO–Al_2O_3–SiO_2–H_2O$ peridotite system at temperatures in the range of 800–1400°C and pressures in the range of 10–25 GPa (Litasov and Ohtani 2003). At lower pressures, the boundaries are shown according to experiments in the $Na_2O–CaO–FeO–MgO–Al_2O_3–SiO_2–H_2O$ peridotite (Fumagalli and Poli 2005). The positions of phase boundaries are also extrapolated, using experimental data in the $MgO–SiO_2–H_2O$ and $MgO–Al_2O_3–SiO_2–H_2O$ systems (Komabayashi 2006). Besides, we show the stability field (melting curve) of ice VII determined by the Raman spectroscopy in the externally

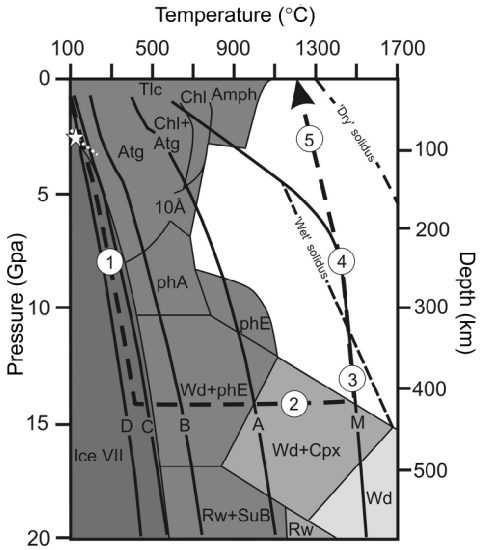

Figure 3. Stability of H_2O-bearing minerals and ice VII to 20 GPa and 1700°C (Litasov and Ohtani 2003; Lin *et al*. 2004; Fumagalli and Poli 2005; Lin *et al*. 2006; Komabayashi 2006). The decreasing degree of shadowing is in decreasing order of water content. Tlc – talc, Chl – chlorite, Amph – amphibole, 10Å – 10-Å phase, Atg – antigorite, phA – phase A, SuB – superhydrous phase B, Wd – wadsleyite, Rw – ringwoodite, and Cpx – clinopyroxene. The stability field of ice VII is superimposed. The star marks the invariant point of ice-II-like and diamond-like $H_2–H_2O$ clathrate structures with corresponding fluid phases (Vos *et al*. 1993). The white dotted line shows the melting curve of the $H_2–H_2O$ clathrate (Vos *et al*. 1993). Methane hydrate is stable at higher temperatures than $H_2–H_2O$ clathrate at a given pressure [for example, about 40°C difference was experimentally observed at 250 MPa (Skiba *et al*. 2007)]. The solid curve marked 'M' is for typical mantle geotherm (Turcotte and Schubert 1992). Other solid curves are for the coldest parts of the four types of subducting slabs, referred to as A, B, C, and D (Bina and Navrotsky 2000). The coldest type D slab represents a fast subduction up to ~20 cm/year. Positions of wet (2 wt.% of H_2O) (Litasov and Ohtani 2003) and dry (Hirschmann 2000) solidus of peridotite-type mantle are shown. The bold dotted curve with numbers in white circles shows the PT path of water recycling within cold subducting slab (1), within stagnant slab (2), and rising water-rich mantle diapir (plume) (3). Crossing the wet solidus at about 300 km depth, the wet rising diapir (plume) starts to melt (4) and melt propagates to the surface (5). These stages are the same as in Figure 2.

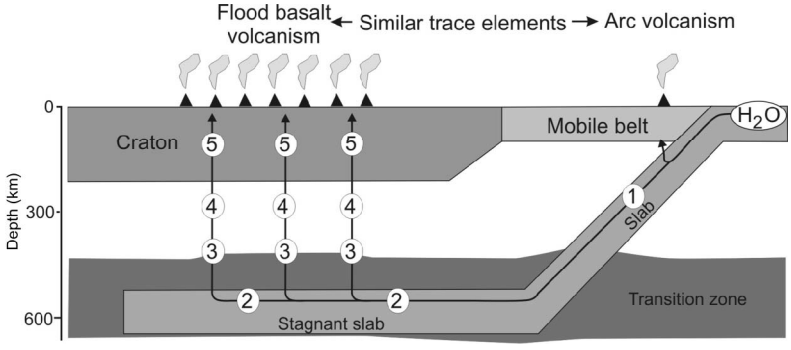

Figure 2. Model of the deep water cycle with slab stagnation in the transition zone (modified after Ivanov *et al*. 2008a). Important stages are numbered (see Figure 3 for explanation).

heated diamond anvil cell (EHDC) (Lin *et al*. 2006). Its position in PT space is in good agreement with the recent experiment on the ice VII melting curve obtained by both Raman spectroscopy and X-ray diffraction in the EHDC (Lin *et al*. 2006; Dubrovinsky and Dubrovinskaia 2007). Irrespective of the experimental results on the melting of ice VII (see Antsyshkin *et al*. 2010 for review of experimental data on high-pressure ice), it remains solid at the coldest slab PT path, as suggested by Bina and Navrotsky (2000) (Figure 3). It has been shown (e.g. Komabayashi 2006) that at a temperature slightly above the melting point of ice VII at a given pressure (along a curve similar to curve B in Figure 3), antigorite undergoes a series of solid–solid transformations to other dense hydrous phases (which, with increasing pressure, are phase A, phase E, superhydrous phase B, and phase D) without loss of its initial water content of about 3.7 wt.%. It is also well known that high-pressure modifications of olivine, wadsleyite, and ringwoodite can accommodate significant amounts of water (up to 3 wt.% in their structures) (e.g. Litasov and Ohtani 2003; Komabayashi 2006). The 10-Å phase may be also important as a water carrier (Wang *et al*. 2004; Fumagalli and Poli 2005; Fumagalli and Stixrude 2007), especially in warmer subduction slabs at the conditions of so-called 'choke point', where severe dehydration melting related to island-arc environments may take place. A new hydrous aluminium (Al) phase similar to pyroxene was synthesized recently at a pressure of 5.4 GPa and at a temperature of 720°C, which can be a carrier of water into mantle beyond the point of chlorite breakdown (Gemmi *et al*. 2011). Another important source of subducting water, which might have been previously underestimated, are clathrate hydrates (gas hydrates) (Vos *et al*. 1993; Skiba *et al*. 2007), which are stable in oceanic sediments, including accretionary prism sediments (e.g. Saito and Suzuki 2007). They do not interact with surrounding sediments and can be accumulated in huge amounts. Subduction of clathrates is questionable, since they have low density relative to the host rocks; however, if their buoyancy force is not high, they can transport much water into the deep mantle. Probably, clathrate hydrates can be crystallized within the peridotitic medium due to reaction of free hydrogen, released at low-temperature serpentinization (Sleep *et al*. 2004), with CO_2. At high pressure, clathrates transform into corresponding ice (VI or VII depending on the pressure). Figure 4 shows that H_2–H_2O and Ar–H_2O clathrates are stable at the PT path of the coldest type D slab at a pressure higher than 1.5 and 3 GPa, respectively. Unfortunately, there are no experimental data on the melting curve at high pressure (above 0.3 GPa) of the most abundant methane hydrate. However, the general rule is that the heavier clathrate hydrates are stable at higher temperatures (Figure 4). Extrapolating available experimental data for methane hydrate and other clathrates allows us to suggest that the methane hydrate should be stable at PT

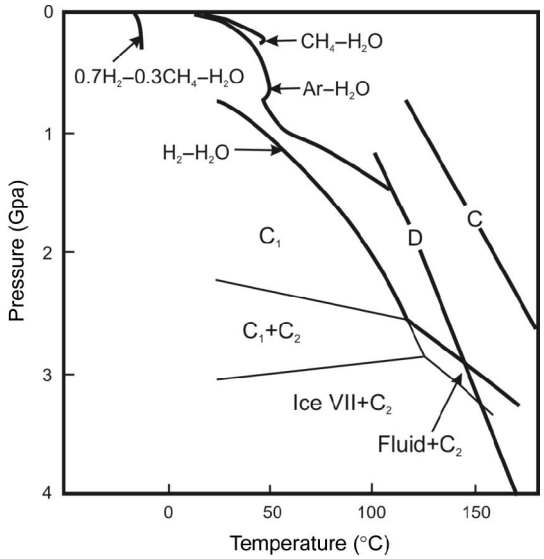

Figure 4. Melting curves of H_2–H_2O, Ar–H_2O, and CH_4–H_2O clathrates (Vos *et al*.1993; Manakov *et al*. 2004; Skiba *et al*. 2007). C_1 and C_2 – crystalline phases of H_2–H_2O, which with increasing pressure transform into ice VII. Curves marked 'C' and 'D' represent PT trends of cold slabs (Bina and Navrotsky 2000). These are the same as in Figure 3.

parameters of cold subducting slabs before its recrystallizing to ice VII. The ice VII, once crystallized is stable down to the transition zone.

There could be probably another way to subduct molecular water in the form of high-pressure ice to the transition zone. It was modelled that upon cooling from the stability field of the 10-Å phase towards the cold subduction geotherm (e.g. D in the Figure 3), molecular water within the crystalline structure was transformed into two-dimensional (2D) rhombohedral ice (Wang *et al*. 2005). With increasing pressure below the stability field of the 10-Å phase, we may expect that the 2D rhombohedral ice will again transform into ice VII.

Summarizing the above statements, there are varieties of H_2O-bearing mineral and crystalline hydrate to ice and mineral to ice reactions which allow the transport of water into the deep mantle by cold slabs (e.g. type D subduction, Figure 3).

Consider now a slab subducting rapidly along the PT path, marked by the bold-dotted curve in Figure 3, or at slightly higher temperatures. In dry conditions, the temperature contrast between the slab and the ambient mantle will ensure that olivine is preserved while crossing the upper mantle–transition zone boundary at about 410 km depth (Bina *et al*. 2001). An olivine-bearing slab in the wadsleyite-dominant transition zone will attain positive buoyancy and deflect to the horizontal (Bina *et al*. 2001). If the slab can pass further through 410 km, it will attain positive buoyancy at the transition zone–lower mantle boundary at about 660 km depth (Bina *et al*. 2001).

Olivine–wadsleyite transformation occurs at a higher speed under the hydrous conditions (e.g. Hosoya *et al*. 2005). Buoyancy of a dominantly dry slab with a hydrated upper part was not modelled numerically. However, irrespective of the modelling it has been well documented in seismic images worldwide that some slabs cannot sink deeper than the transition zone (e.g. Fukao *et al*. 2001, 2009), but they move horizontally as long as the subduction continues without break-off of the slab (alternatively, the slab can be fixed while the lithospheric plate runs over it; the effect remains the same, i.e. the stagnant slab propagates beneath inner continental parts) (Zorin *et al*. 2006; Faccenna *et al*. 2010). This effect is known as slab stagnation. With time, the stagnant slab will heat up to the temperature of the ambient mantle along the horizontal part of the bold-dotted curve in Figure 3. With increasing temperature, phase E will decompose to wadsleyite and fluid, and then wadsleyite gradually lose its water to produce free H_2O-bearing fluid (Figure 3). This fluid will rise to a 410 km discontinuity, where it can be accumulated in the dense hydrous melt up to an appropriate amount (Bercovici and Karato 2003; Sakamaki *et al*. 2006). If water is subducted as the solid ice VII, the above scenario of course remains valid and the effect of the deep water cycle will be more prominent.

In the lowermost upper mantle, water can be completely dissolved in the olivine structure if the total amount of H_2O does not exceed the water-capacity of the olivine at that depth (the preferred estimate of which is about 0.5–0.6 wt.% at a temperature of 1200°C and pressure in the range of 12–14 GPa) (Hirschmann *et al*. 2005; Smyth *et al*. 2006; Litasov *et al*. 2007; Litasov 2011). The addition of 0.5 wt.% of water to the olivine structure has the same effect on the olivine volume by increasing the temperature by 240°C (Smyth *et al*. 2006). Thus, release of water from the stagnant slab is equivalent to heating the mantle above by a value considered sufficient for a thermally buoyant mantle plume (e.g. Campbell and Griffiths 1990). A water-driven mantle plume will rise by its own buoyancy and melt on crossing its wet solidus beneath thick cratonic lithosphere (Figure 3). Such a water cycle, linked to cold subduction, slab stagnation, and wet plume rising, is expected to result in magmatism similar to that seen in island-arc systems, but at larger distance from a trench and induced by slab dehydration at greater depths (Figure 2) (Ivanov *et al*. 2008a).

Modelling PT trends for subducting slabs

Kirby *et al*. (1996) subdivided subducting slabs in the order from hot to cold into the four major types A, B, C, and D. The coldest type D slab represents subduction of 140 Ma oceanic slab at a rate of 14 cm/year and at an angle of 60° (e.g. Tonga slab) (Kirby *et al*. 1996). GPS measurements of the convergence rate in the northern part of the Tonga plate show that it may be between 16 and 24 cm/year depending on the selected coordinate system (Bevis *et al*. 1995). Type C is characterized by a slower subduction rate of 8 cm/year and the same other parameters as for the D type such as the slab age and angle of subduction (e.g. Kuril slab). Type B represents subduction of 50 Ma oceanic plate at 45° angle and at a rate of 7 cm/year (e.g. subduction under Latin America). Type A is the subduction of a young oceanic plate at 30° angle and at a rate of 5 cm/year (e.g. subduction under Mexico). There have been a number of attempts to model PT trends for subducting slabs (e.g. Kirby *et al*. 1996; Bina and Navrotsky 2000; Van Keken *et al*. 2002; Negredo *et al*. 2004; Arcay *et al*. 2007; Syracuse *et al*. 2010). Despite the different approaches, the essence of these calculations for our study is that old quickly subducting slabs are cold enough to bring H_2O-bearing minerals into deep mantle both within oceanic crust and within peridotite.

Bina and Navrotsky (2000) modelled PT trends for the four types of slabs using a standard kinematic finite difference method (Toksoèz *et al*. 1973) and yielded a conclusion that the coldest D-type slab is cold enough to bring water into deep mantle in the form of high-pressure ice VII. To verify this conclusion, we computed PT parameters for the D-type slab using the thermo-kinematic algorithm of Negredo *et al*. (2004), which accounts for adiabatic heating and heating resulting from major phase transitions and shearing. For initial distribution of the temperature within the subducting plate, a model similar to the global depth and heat flow (GDH1) model (Stein and Stein 1992) was applied, but the temperature at the base of the lithosphere was set up to be 1350°C. For example, Bina and Navrotsky (2000) used two models with temperatures of 1450°C and 1325°C at the base of the lithosphere. PT trends for the D-type slab after Bina and Navrotsky (2000) and the algorithm of Negredo *et al*. (2004) overlap within the line thickness shown in Figure 3. These results are also in good agreement with other models. For example, Syracuse *et al*. (2010) calculated for the Tonga slab a minimum temperature of 265°C at 240 km depth, which is plotted at the PT curve for the D-type slab shown in Figure 3.

It is important to note that within the D-type slab a wedge of metastable olivine should be formed (Figure 5). At the mantle transition zone depths, olivine has lower density compared to that of wadsleyite, which creates positive buoyancy forces within the slab. As seen from Figure 5, there is a wedge of positive buoyancy at a depth interval of ~470–550 km in the central part of the D-type slab, whereas the bottom of the slab is anomalously dense at a depth interval of ~350–450 km. Combination of these two positive and negative buoyancy regions leads to the slab gentling and stagnation in the transition zone. This is in good agreement with the modelling reported elsewhere (e.g. Bina *et al*. 2001).

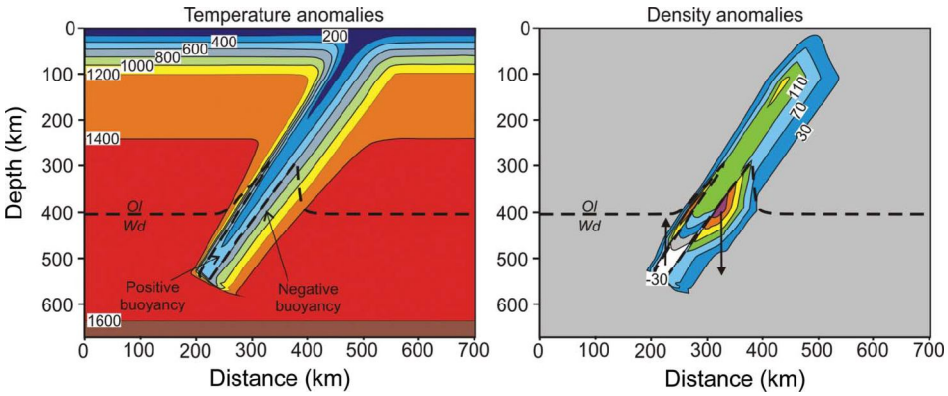

Figure 5. Temperature and density anomalies within the D-type slab of Kirby *et al*. (1996) modelled using the MATLAB algorithm of Negredo *et al*. (2004). The following parameters were used for the calculation: thermal conductivity coefficient 3.2 W/mK, heat capacity coefficient 1.3×10^3 J/kgK, thermal expansion coefficient 3.7×10^{-5} $1/K$, mantle density 3400 kg/m^3, olivine-wadsleyite density jump 181 kg/m^3, and latent heat of the olivine–wadsleyite transition -9×10^{-4} J/kg. Numbers show the temperature in °C and the density in kg/m^3 compared to ambient mantle density at the same depth. Thin arrows in the left figure point to the regions of anomalously positive and negative buoyancy. Thick arrows in the right figure indicate the direction of buoyancy forces originating in the slab.

Mineralogical evidence for deep water cycle

It would be extremely difficult to find H_2O-bearing minerals such as phase A, phase D, and super-hydrous phase B in nature, because they quickly become amorphous at a temperature of about 100−300°C and at a pressure of 1 atm (Williams and Hemley 2001). In other words, the probability that these phases can be preserved during the way up to the surface is very low even if they were initially trapped as inclusions in a diamond. There are findings of CH_4-H_2O fluid inclusions in olivines of mantle peridotites (Liu and Fei 2006), which could be stable as methane hydrate in a cold subduction environment. However, such findings cannot be taken as a proof for subduction of water in the form of methane hydrate. At mantle depth and expected oxygen fugacity, fluid becomes rich in water and methane if carbon and hydrogen are available in the fluid. Anyway, breakthrough results have been achieved recently in discovering H_2O-bearing minerals in diamond inclusions, which could be stable only at lower upper mantle and/or transition zone depths. For example, phase Egg and topaz-OH have been discovered as nanometric size inclusions in diamonds from Erzgebirge ultrahigh pressure complex (Dobrzhinetskaya *et al*. 2007). Phase Egg in association with transition zone minerals has also been discovered in diamonds of Juina in Brazil (Wirth *et al*. 2007). Phase-10Å, serpentine, and talc have been discovered in a peridotitic assemblage as lamellas in olivines sampled from kimberlites of Yakutia and South Africa (Khisina and Wirth 2008; Khisina *et al*. 2008). Thus, there is direct evidence for subduction of water into deep upper mantle and into the transition zone via cold slabs.

Trace-element signatures of deep water cycle

The effect of water on trace elements in subduction systems is well understood; water carries, from dehydrating slabs, large-ion lithophile elements such as Ba, K, and Sr, and light rare earth elements such as La, but it is not able to carry high field strength elements such as Ti and Nb (e.g. McCulloch and Gamble 1991; Portnyagin *et al*. 2007). It also fractionates Th and U (e.g. McCulloch and Gamble 1991; Portnyagin *et al*. 2007). High-degree partial melting of the water-saturated source above subducting slabs yields magmas with typical island-arc basalt trace-element patterns with low high-field-strength- and high large-ion-lithophile-element abundances and depletion of Th relative to U.

The Siberian flood basalt province with its dominant low-Ti basalt type (Fedorenko *et al*. 1996) and the 'subduction' trace-element fingerprints (Puffer 2001) lay in a back-arc of the Mongolia–Okhotsk subduction (Enkin *et al*. 1992; Van der Voo *et al*. 1999; Zorin 1999) at the time of flood basalt eruption (Nikishin *et al*. 2002; Ivanov 2007; Ivanov *et al*. 2013) (Figure 6). Subduction from the south (in present-day coordinates) beneath Siberia has been documented from the Devonian until the closure of the Mongolia–Okhotsk Ocean in the Late Triassic (Donskaya *et al*. 2013), Late Jurassic (Zorin 1999), or Early Cretaceous (Van der Voo *et al*. 1999). Siberian flood basalt magmatism had two pulses at the Permo–Triassic boundary and in the Middle Triassic, but accompanied felsic magmatism lasted as long as 22–26 million years from the late Permian until the Middle Triassic as shown by U–Pb and $^{40}Ar/^{39}Ar$ geochronologic data (Ivanov *et al*. 2013). Overall, long duration is independently supported by palaeomagnetic data (Steiner 2006). Palaeotectonic reconstruction of subduction beneath the Siberian part of Pangea in Permo-Triassic time (Enkin *et al*. 1992), which is the time of the major pulse of the Siberian Traps flood basalt emplacement (Renne and Basu 1991; Kamo *et al*. 2003), is shown in Figure 6. Similar palaeotectonic reconstructions can be found elsewhere (Van der Voo *et al*.

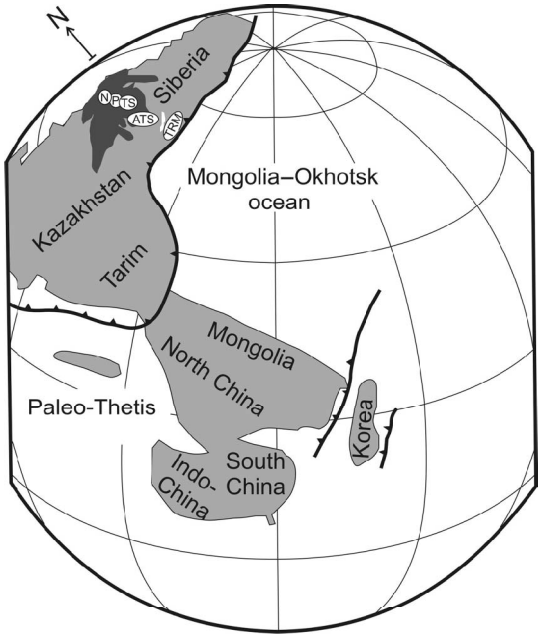

Figure 6. Palaeotectonic reconstructions of the Mongolia–Okhotsk Ocean and its surroundings in Permo-Triassic time (Enkin *et al*. 1992). Bold curves mark subduction zones. The coeval Siberian Traps flood basalt province is shown in dark grey. The arrow indicates present-day north for Siberia. White circles indicate localities discussed in the text: from present-day south to north they are Transbaikalian-rifted margin (TRM), Angara–Taseevskaya syncline (ATS), Tunguska syncline (TS), Putorana (P), and Noril'sk (N).

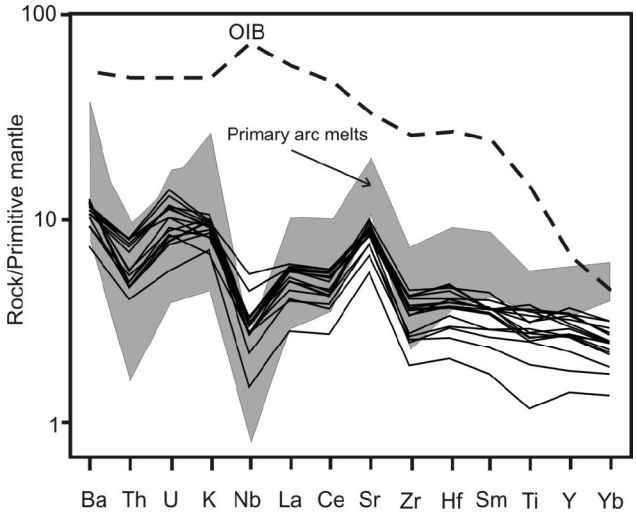

Figure 7. Primitive mantle (Sun and McDonough 1989) normalized diagram for initial melts of the Angara–Taseevskaya syncline (bold lines). Original measured compositions (Ivanov *et al*. 2008a, 2009) were recalculated (corrected) to the initial melt compositions by adding olivine and plagioclase (Table 2). The shaded field represents the compositional range of the primary melts of the modern arc of the Eastern Kamchatka (Portnyagin *et al*. 2007). The modelled primary basaltic melt composition of ocean islands (OIB after Sun and McDonough 1989) is drastically different from those of the Angara–Taseevskaya syncline.

1999; Zorin 1999; Nikishin *et al*. 2002). Remnants of the Mongolia–Okhotsk slab are probably recognizable in seismic tomography images beneath Siberia (Van der Voo *et al*. 1999).

Figure 7 shows trace-element patterns of the Early-to-Middle Triassic dolerite sills in the Angara–Taseevskaya syncline, which belongs to the southeastern (in present-day coordinates) Siberian flood basalt province. It has been shown that trace-element variations in the sills are explained largely by the olivine and plagioclase fractionation (Ivanov *et al*. 2008a). Thus, the original data for rocks are recalculated back to their initial melt compositions using the equilibrium fractionation of olivine and plagioclase according to the following equation:

$$C_{\text{measured}} = C_{\text{initial}}/(D + F - DF), \quad (1)$$

where C_{measured} and C_{initial} are the concentrations of elements in question measured in the rock sample and initial melt prior to fractionation, respectively, F is a fraction of remaining melt, and D is a bulk distribution coefficient,

$$D = x_i D_i + x_j D_j, \quad (2)$$

where x_i and x_j are the fractions of the crystallizing minerals (in our case these are the olivine and plagioclase), and D_i and D_j are their distribution coefficients (Shaw 1970).

Mg-number [$Mg/(Mg + 0.85Fe_{total})$] and Sr/Pr were used as proxies to estimate the fractions of crystallized olivine and plagioclase, respectively. Distribution coefficients for Sr, Pr, and other elements are listed in Table 1. For olivines, $D^{Mg/Fe} = 2.8$ was used. Measured and recalculated concentrations are listed in Table 2.

Table 1. Mineral/melt distribution coefficients after (Dun and Sen 1994). Asterisks mark extrapolated values.

Element	Olivine/melt	Plagioclase/melt
Ti	0.015*	0.037
K	0.003*	0.9*
Sr	0.012	2.4
Y	0.029	0.012
Zr	0.015*	0.0002
Nb	0.004	0.024
Ba	0.001*	0.69
La	0.0001*	0.12
Ce	0.024	0.097
Pr	0.031	0.077
Sm	0.016	0.048
Yb	0.053	0.0098
Hf	0.02	0.08
Th	0.01*	0.064
U	0.01*	0.078

Table 2. Selected major (wt.%) and trace elements (ppm) for dolerites of the Angara–Taseevskaya syncline (Ivanov *et al*. 2008a, 2009) and recalculated initial melt compositions (this work). Mg# – Mg-number.

Sill	Tolstomysovsky							
Sample	833		834		847		851	
	Measured	Initial	Measured	Initial	Measured	Initial	Measured	Initial
Mg#	40	68	35	68	56	68	58	68
TiO_2	1.64	0.39	1.74	0.24	1.00	0.53	0.96	0.63
K_2O	0.79	0.28	0.79	0.20	0.41	0.27	0.41	0.31
Sr	203	132	192	110	190	165	195	176
Y	33	7.7	44	6.1	22	12	22	15
Zr	117	27	153	20	74	39	67	44
Nb	6.3	1.4	7.6	1.0	3.5	1.8	3.3	2.1
Ba	188	61	220	49	114	70	102	73
La	11	2.7	13	1.8	6.7	3.6	5.6	3.7
Ce	25	6.1	31	4.6	16	8.6	14	9.3
Sm	4.0	0.95	5.1	0.70	2.8	1.5	2.2	1.5
Yb	3.1	0.76	4.1	0.60	2.1	1.1	1.9	1.2
Hf	3.1	0.74	4.1	0.58	2.1	1.1	1.9	1.3
Th	1.8	0.42	2.4	0.32	1.2	0.64	0.91	0.60
U	0.66	0.16	0.82	0.11	0.39	0.21	0.35	0.23
Sill	Tolstomysovsky							
Sample	887		888		891		3A	
	Measured	Initial	Measured	Initial	Measured	Initial	Measured	Initial
Mg#	69	69	68	68	65	68	51	69
TiO_2	0.74	0.73	0.71	0.71	0.79	0.68	1.59	0.56
K_2O	0.28	0.28	0.27	0.27	0.31	0.28	0.46	0.24
Sr	168	167	177	177	187	179	227	193
Y	15	15	15	15	16	14	36	13
Zr	45	45	43	43	51	44	115	40
Nb	2.0	2.0	2.1	2.1	2.5	2.2	5.9	2.0
Ba	71	70	77	77	86	76	171	80
La	3.6	3.6	3.7	3.7	4.4	3.8	9.4	3.4
Ce	9.0	8.8	9.1	9.1	11	9.5	20	7.4
Sm	1.5	1.5	1.6	1.6	1.7	1.5	4.2	1.5
Yb	1.2	1.2	1.4	1.4	1.5	1.3	3.0	1.1
Hf	1.4	1.3	1.2	1.2	1.6	1.4	3.0	1.1
Th	0.56	0.55	0.64	0.64	0.73	0.63	1.1	0.39
U	0.24	0.24	0.23	0.23	0.30	0.26	0.51	0.18
Sill	Chuna-Biryusinsky		Padunsky		Tulunsky		Usol'sky	
Sample	38–28		9/114y		T2		2843	
	Measured	Initial	Measured	Initial	Measured	Initial	Measured	Initial
Mg#	47	70	48	70	49	68	43	68
TiO_2	1.80	0.53	1.64	0.51	1.49	0.63	1.89	0.59
K_2O	0.57	0.26	0.53	0.25	0.43	0.23	0.45	0.20
Sr	240	193	229	184	252	199	212	150
Y	40	12	37	12	37	16	37	12
Zr	133	38	123	38	114	47	95	29
Nb	6.4	1.8	5.9	1.8	5.3	2.2	6.1	1.9
Ba	203	82	190	81	156	80	153	61
La	11	3.2	10	3.2	8.5	3.7	9.2	2.9
Ce	23	7.2	22	7.1	19	8.3	22	7.1
Sm	4.8	1.4	4.4	1.4	4.2	1.8	3.7	1.2
Yb	3.6	1.1	3.1	1.0	3.3	1.4	3.0	0.97
Hf	3.5	1.1	3.3	1.1	3.0	1.3	3.0	0.95
Th	1.3	0.37	1.2	0.37	1.1	0.44	1.3	0.39
U	0.56	0.17	0.48	0.15	0.49	0.21	0.54	0.17

(*Continued*)

Table 2. (Continued).

Sill	Usol'sku							
Sample	2845		2847		2848		2854	
	Measured	Initial	Measured	Initial	Measured	Initial	Measured	Initial
Mg#	46	70	43	70	50	68	49	68
TiO_2	1.90	0.55	2.18	0.50	1.83	0.77	1.76	0.72
K_2O	0.64	0.29	0.72	0.28	0.48	0.26	0.53	0.28
Sr	209	168	194	151	227	180	219	172
Y	39	11	41	9.5	32	9.5	31	13
Zr	99	28	116	26	86	26	88	36
Nb	7.2	2.1	8.1	1.8	7.1	2.9	8.8	3.6
Ba	192	78	195	68	137	70	147	74
La	11	3.2	10.7	2.6	8.8	3.8	9.4	3.9
Ce	25	7.6	26	6.4	21.2	9.2	23	95
Sm	4.0	1.2	4.6	1.1	3.5	1.5	3.6	1.5
Yb	3.2	0.95	3.4	0.82	2.6	1.1	2.6	1.1
Hf	2.8	0.84	3.5	0.83	2.5	1.1	2.7	1.2
Th	1.5	0.45	1.6	0.37	1.4	0.58	1.6	0.64

Table 3. Average PGE and Re compositions (ppb) for the Angara–Taseevskaya dolerites and volcanic rocks of various tectonic settings.

	Os	Ir	Ru	Pt	Pd	Re
Angara–Taseevskaya dolerites (Ivanov *et al*. 2009)	0.14	0.12	0.50	14.2	19.8	0.60
Low-K basalts of Kamchatka (Ivanov *et al*. 2008c)	0.50	0.09	0.46	4.5	21.8	0.39
Tholeiites and pictrites of Hawaii (Benett *et al*. 2000; Crocket 2000; Jamais *et al*. 2008)	0.38	0.35	0.63	3.4	2.7	0.54
Intra-continental alkaline basalts (Holocene, East Sayan, Siberia) (Ivanov *et al*. 2008b)	0.04	0.01	0.03	0.70	0.06	0.12

The initial melt compositions of the southeastern Siberian flood basalt province are remarkably similar to the initial melt compositions of the modern arc of the Eastern Kamchatka (Portnyagin *et al*. 2007), suggesting a similar model for their origin in relation with dehydration of subducting slabs (Figure 7). These testify that the deep water cycle played an important role in the origin of initial melts of the southeastern Siberian flood basalt province despite it being located about 700 km away from the expected subduction trench.

If platinum group elements (PGE) are considered (Table 3), dolerite sills of the southeastern Siberian flood basalt province are similar to the particular low-K type of arc basalts of Kamchatka (Figure 8), though platinum group elements may not be useful as trace elements for distinguishing between arc basalts and flood basalts on one hand and ocean island basalts on the other hand.

To assess the role of the deep water cycle on more remote regions of the Siberian flood basalt province, we plot the Nb/La ratio as a function of distance from the Mongolia–Okhotsk suture zone, which can be viewed as a distance from subduction trench. The Nb/La ratio is taken because it is not affected by the olivine and plagioclase fractionation. From Figure 9, it can be seen that the Nb/La ratio gradually increases from the typically low island-arc values (Portnyagin *et al*. 2007) in proximity to the

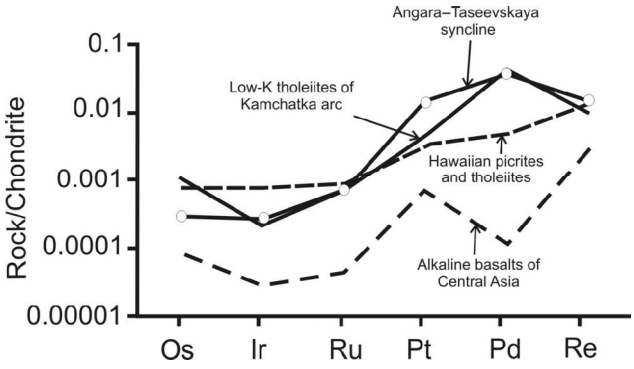

Figure 8. Comparison of average chondrite normalized (McDonough and Sun 1995) PGE spectra for dolerites of the Angara–Taseevskaya syncline (Ivanov *et al*. 2009), low-K Kamchatka-arc tholeiites (Ivanov *et al*. 2008c), Holocene alkaline basalts from the East Sayan Mountains of Central Asia (Ivanov *et al*. 2008b) and Hawaiian picrites and tholeiites (Bennett *et al*. 2000; Crocket 2000; Jamais *et al*. 2008) (see Table 3).

Mongolia–Okhotsk subduction system towards typically high ocean island basalt values (Sun and McDonough 1989) at Noril'sk, showing the decreasing influence of subduction on the trace-element budget of the flood basalts and the increasing role of within plate-type source (delamination or plume).

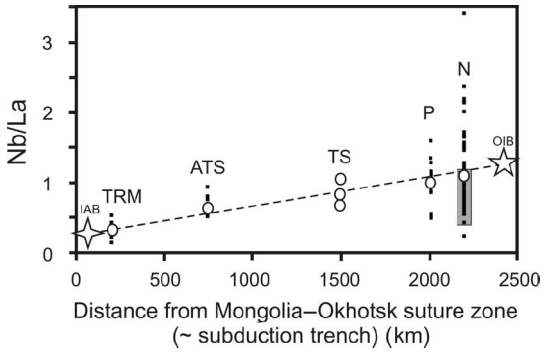

Figure 9. Nb/La variations in basaltic rocks from the rifted margin of Siberia through the Siberian flood basalt province. MOSZ – Mongolia–Okhotsk suture zone, which represents the boundary between the Siberian and Mongolian terranes (Enkin *et al*. 1992) and can be considered as the approximate position of the trench at the time of subduction of the Mongolia–Okhotsk slab (Figure 6). Original Nb/La ratios (Wooden *et al*. 1993; Ryabchikov *et al*. 2001; Yarmolyuk *et al*. 2001; Al'mukhamedov *et al*. 2004; Ivanov *et al*. 2008a, 2009; Sobolev *et al*. 2009) (not recalculated to crystal fractionation) are plotted. This ratio was chosen because it is least affected by the olivine and plagioclase fractionation compared to other key trace-element ratios for defining subduction setting *versus* within-plate setting (e.g. K/Nb, Sr/Pr, and Ce/Pb). Small black squares are for individual samples. Large white circles are for average compositions. For the Tunguska syncline, only the average compositions of three large lava units were published (Al'mukhamedov *et al*. 2004). The grey rectangle for Noril'sk is the range of Nb/La ratios after Sobolev *et al*. (2009). IAB – island-arc basalts (Portnyagin *et al*. 2007). OIB – ocean island basalts (Sun and McDonough 1989). The dashed line connects IAB and OIB for eye guiding. Other acronyms as in Figure 6.

Discussion

The size and volume of the Siberian flood basalt province is enormous. The size is almost the same as the present-day Australian continent and the most reliable estimations of the volume are close to 4×10^6 km^3; neither can easily be explained by any model, and this includes the plume model in its classic form (see Ivanov 2007 for review). Having this in mind, it would be worth considering alternative models for the origin of the Siberian flood basalt volcanism.

Usually, various lower mantle plume models are invoked. In the classic model (Griffiths and Campbell 1990; Campbell and Griffiths 1990), the lower mantle plume is essential to explain the size of the Siberian flood basalt province by the plume head, where size is increasing during the plume uprising. However, the actual size of the Siberian flood basalt province (~4000 km in diameter) is significantly larger compared to the modelled 1000 km in diameter (e.g. Sobolev *et al*. 2011). Originally, in the frame of the plume model, it was suggested that the volcanism should be preceded by domal uplift (Campbell 2005), which is known to be non-existent however (Czhamanske *et al*. 1998). Later, it was argued that the domal uplift is unnecessary (Burov and Guillou-Frottier 2005), compensated by dense eclogite in the plume (Sobolev *et al*. 2011), or the plume volcanism should be preceded by subsidence (Leng and Zhong 2010). Observed pre-volcanic subsidence and later uplifting (Czhamanske *et al*. 1998) fits expectations of catastrophic thinning of the lithosphere via Rayleigh–Taylor controlled delamination better than the plume model (Elkins-Tanton 2005). The model of catastrophic lithospheric thinning has problems in explaining the size of the Siberian flood basalt province, which as was mentioned before is comparable to the Australian continent.

Using geochemical arguments, Sobolev *et al*. (2007, 2009a) suggest that the plume contained eclogite. Eclogite has a lower melting temperature compared to peridotite. It melts producing dacitic magma. The dacitic magma reacts with peridotitic mantle forming a hybrid pyroxenite source. The pyroxenite in its turn melts producing tholeiitic magma (Sobolev *et al*. 2007, 2009). However, in the case of the Siberian flood basalts, Sobolev *et al*. (2009) assumed unrealistically thin lithosphere of about 130 km thick (Figure 10A). Nuclear explosion seismic studies suggest that the lithosphere is 180–220 km thick beneath different parts of Siberia (Pavlenkova and Pavlenkova 2006), and similar results for the lithospheric thickness were obtained using surface wave tomography (Priestley and McKenzie 2006; Pasyanos 2010) and it is unlikely that the lithosphere was significantly thinner in Permo-Triassic time (Zorin and Vladimirov 1989). With 180–220 km-thick lithosphere, volatile-free pyroxenite cannot be melted at any reasonable potential temperature of the plume. The deep water cycle model resolves this problem because the solidus of the water-rich plume, let us denote it as 'diapir' to distinguish it from the lower mantle plume, is much lower and allows melting of mantle below thick cratonic lithosphere at a normal mantle geotherm or at a modest elevated temperature (Figure 10B).

It is worth mentioning that the deep water cycle does not rule out the possibility of oceanic crust recycling (eclogite), because mantle diapirs starting from the transition zone can bring dense eclogitic material (Yasuda and Fujii 1998). Modelling in subduction zones shows that two types of diapir (plume) may be initiated: unmixed due to fluid infiltration to peridotite and mixed due to mixing of slab and peridotite material (Gerya *et al*. 2006). Indeed geochemical and isotopic variations in lavas of the Noril'sk region require involvement of both peridotitic mantle and eclogitic material (Ivanov 2007; Sobolev *et al*. 2009a).

The deep water cycle model also gives good explanation for findings of primary magmatic amphibole and phlogopite in intrusions of the Siberian flood basalt province (Ivanov *et al*. 2008a), the fact which was overlooked when previous studies were focused on high temperature instead of lower melting point due to hydrated source.

Other possibilities should be considered in future studies, bearing in mind the decreasing influence of subduction on the most remote regions of the Siberian flood basalt

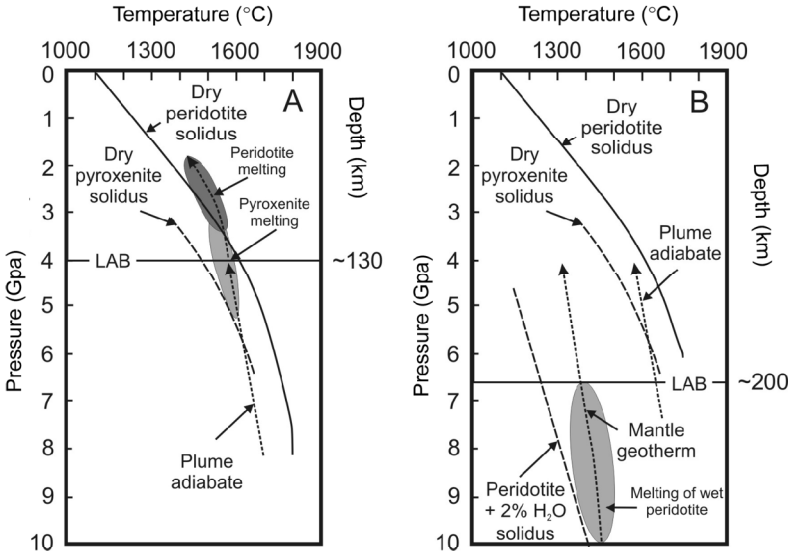

Figure 10. Two different models for the origin of the Siberian flood basalts; A (Sobolev *et al*. 2009a, 2011) and B (Ivanov *et al*. 2013). In model A, melting is assumed to start within the pyroxenitic source, which originated due to melting of plume-entrained eclogite and eclogite-derived melt reaction with peridotitic matrix within the plume column (reproduced after Sobolev *et al*. 2009a). Peridotitic mantle starts to melt due to lithospheric delamination (Sobolev *et al*. 2011). However, this model uses unrealistically thin lithosphere for the Siberian craton. If lithospheric thickness of about 200 km is accounted for then the sub-lithospheric melting of the pyroxenite source became impossible at a reasonable temperature of a plume (see B). Our model involves a wet plume (diapir) whose solidus is much lower compared to that of a dry pyroxenite solidus. This allows melting underneath the 200 km-thick lithosphere. Our model allows entraining eclogite from the stagnant slab into the wet plume (diapir) as modelled by Yasuda and Fujii (1998). So, the two-stage model of Sobolev *et al*. (2009a, 2011) with melting of pyroxenite and peridotite sources remains valid but at higher depth due to the wetter plume (diapir).

province (Figure 9) or, for example, the increasing evidence for the essential role of subducted carbonates in the upper mantle dynamics (e.g. Litasov *et al*. 2013). Probably, there were two important factors in the origin of the Siberian flood basalts: lower mantle plume and hydrated transition zone. In this case, the unique size and volume of the Siberian flood basalt province is due to the coexistence of two forces: high temperature from the plume and low melting temperature from the upper mantle hydration via the deep water cycle. However, it is not impossible that the size of the Siberian flood basalt province is solely due to long-term subduction beneath Siberia (Donskaya *et al*. 2013).

Unresolved questions

The model described here is logical and can account of many geological facts about the Siberian flood basalt province. For example, the location is predicted from the direction of slab subduction, the great size is due to the size of the subducted slabs, the volume is due to the flux-supported volumetric melting, the short pulses are due to the pulses of solid ice melting and thus creation of wet diapirs, depletion in Nb, Ta, and Ti is due to the immobility of these elements within water fluid, etc. However, some unresolved questions remain. Such are flat trace-element spectra for dominant low-Ti basalts showing no garnet signature, which is expected from great depth of melting in our model. This could be explained in principle by a high degree of partial melting when garnet is no longer a residual phase. But, this is a purely hypothetic explanation at the moment. Another unresolved question is that nobody has found so far excess water in the melt inclusions (Sobolev *et al*. 2009b; Panina and Motorina 2013), despite that the prediction of our model would be water content in excess of 2 wt.% or maybe up to 4 wt.% (which are typical values for arc magmas).

Conclusions

Experimental data and numerical calculations suggest that in the case of fast (cold) subduction (~20 cm/year), serpentine formed within the peridotitic part of an oceanic slab can transport a significant amount of water into mantle beyond the shallow sub-arc depth of slab degassing. With depth, serpentine transforms into high-pressure phases, which devolatilize only in the mantle transition zone after a temporal delay, which is essential for the slab warming. After slab devolatilization in the transition zone, wet buoyant plumes (diapirs) are generated. Such diapirs rise and undergo decompression melting at a depth of about 200 km. That is the driving force for flood basalt volcanism. Such H_2O cycling is named here the deep water cycle. It is also possible that H_2O can be subducted in the form of high-pressure ice. If so, the deep water cycle model and its connection to the flood basalt volcanism is strengthened.

The Siberian flood basalt province formed in a far back-arc region of the Mongolia–Okhotsk subduction system. The areas least remote from the subduction zone are characterized by the presence of magmatic rocks, whose geochemical features resemble typical arc tholeiites. This resemblance gradually declines with increasing distance from the subduction zone, thus showing a decreasing role of underflow for the most remote areas of the flood basalt province. Accordingly, the unique size and volume of the Siberian flood basalts may reflect long-term subduction beneath Siberia with or without the participation of a lower mantle plume.

Acknowledgements

The manuscript was initiated by three consequent presentations given by A.V.I. at the Institute of Geology and Geophysics of the Chinese Academy of Sciences (Beijing, China), Institute of the Earth's Crust of the Siberian Branch of the Russian Academy of Sciences (Irkutsk, Russia), and Institute of Earth Science Academia Sinica (Taipei, Taiwan). It benefited from questions and discussions during and after the presentations and from intensive discussions and critiques from colleagues. We particularly thank Alex Sobolev for his strong criticism, which stimulated us to search for stronger arguments. The work was completed during the Fulbright Scholarship of A.V.I. at the Department of Earth Sciences, University of New Hampshire. The work of K.D.L. was supported by the Ministry of Education and Science of the Russian Federation, project No. 14.B25.31.0032.

References

Al'mukhamedov, A.I., Medvedev, A. Ya., and Zolotukhin, V.V., 2004, Chemical evolution of the Permian-Triassic basalts of the Siberian platform in space and time: Petrology, v. 12, p. 297–311.

Antsyshkin, D.V., Dunaeva, A.N., and Kuskov, O.L., 2010, Thermodynamics of phase transitions in the system ice VI – ice VII – water: Geochemistry International, v. 48, p. 633–642.

Arcay, D., Doin, M.-P., Tric, E., and Bousquet, R., 2007, Influence of postcollisional stage on subduction dynamics and the buried crust thermal state: Insights from numerical simulations: Tectonophysics, v. 441, p. 27–45.

Bennett, V.C., Norman, M.D., and Garcia, M.O., 2000, Rhenium and platinum group element abundances correlated with mantle source components in Hawaiian picrites: Sulphides in the plume: Earth and Planetary Science Letters, v. 183, p. 513–526.

Bercovici, D., and Karato, S.-I., 2003, Whole-mantle convection and the transition-zone water filter: Nature, v. 425, p. 39–44.

Bevis, M., Taylor, F.M., Schutz, B.E., Recy, J., Isaks, B.L., Helu, S., Singh, R., Kendrick, E., Stowell, J., Taylor, B., and Calmant, S., 1995, Geodetic observations of very rapid convergence and back-arc extension at the Tonga arc: Nature, v. 374, p. 249–251.

Bina, C.R., and Navrotsky, A., 2000, Possible presence of high-pressure ice in cold subducting slabs: Nature, v. 408, p. 844–847.

Bina, C.R., Stein, S., Marton, F.C., and Van Ark, E.M., 2001, Implications for slab mineralogy for subduction dynamics: Physics of Earth and Planetary Interiors, v. 127, p. 51–66.

Burov, E., and Guillou-Frottier, L., 2005, The plume head-continental lithosphere interaction using a tectonically realistic formulation for the lithosphere: Geophysical Journal International, v. 161, p. 469–490.

Campbell, I.H., 2005, Large igneous provinces and the mantle plume hypothesis: Elements, v. 1, p. 265–270.

Campbell, I.H., and Griffiths, R.W., 1990, Implications of mantle plume structure for the evolution of flood basalts: Earth and Planetary Science Letters, v. 99, p. 79–93.

Crocket, J.H., 2000, PGE in fresh basalt, hydrothermal alteration products, and volcanic incrustations of Kilauea volcano, Hawaii: Geochimica et Cosmochimica Acta, v. 64, p. 1791–1807.

Czamanske, G.K., Gurevich, A.B., Fedorenko, V., and Simonov, O., 1998, Demise of the Siberian plume: paleogeographic and paleotectonic reconstruction from the prevolcanic and volcanic records, North-Central Siberia: International Geology Review, v. 40, p. 95–115.

Dobrzhinetskaya, L.F., Wirth, R., and Green II, H.W., 2007, A look inside of diamond-forming media in deep subduction zones: Proceedings of National Academy of Science, v. 29, p. 9128–9132.

Donskaya, T.V., Gladkochub, D.P., Mazukabzov, A.M., and Ivanov, A.V., 2013, Late Paleozoic–Mesozoic subduction-related magmatism at the southern margin of the Siberian continent and the 150-million-year history of the Mongolia-Okhotsk Ocean: Journal of Asian Earth Sciences, v. 62, p. 79–97.

Dubrovinsky, L., and Dubrovinskaia, N., 2007, Melting of ice VII and new high-pressure high-temperature amorphous ice, *in* Ohtani, E., ed., Advances in high-pressure mineralogy: Geological Society of America Special Paper, v. 421, p. 105–114.

Dun, T., and Sen, C., 1994, Mineral/matrix partition coefficients for orthopyroxene, plagioclase, and olivine in basaltic to andesitic systems: A combined analytical and experimental study: Geochimica et Cosmochimica Acta, v. 58, p. 717–733.

Enkin, R.J., Yang, Z., Chen, Y., and Courtillot, V., 1992, Paleomagnetic constraints on the geodynamic history of major blocks of China from the Permian to the present: Journal of Geophysical Research, v. 97, p. 13953–13989.

Faccenna, C., Becker, T.W., Lallemand, S., Lagabrielle, Y., Funiciello, F., and Piromallo, C., 2010, Subduction-triggered magmatic pulses: A new class of plumes? Earth and Planetary Science Letters, v. 299, p. 54–68.

Fedorenko, V.I., Lightfoot, P.C., Naldrett, A.J., Czamanske, G.K., Hawkesworth, C.J., Wooden, J.L., and Ebel, D.S., 1996, Petrogenesis of the flood-basalt sequence at Noril'sk, North Central Siberia: International Geology Review, v. 38, p. 99–135.

Fukao, Y., Obayashi, M., and Nakakuki, T., 2009, Stagnant slab: a review: Annual Review of Earth and Planetary Sciences, v. 37, p. 19–46.

Fukao, Y., Widiyantoro, S., and Obayashi, M., 2001, Stagnant slabs in the upper and lower mantle transition region: Reviews of Geophysics, v. 39, p. 291–323.

Fumagalli, P., and Poli, S., 2005, Experimentally determined phase relations in hydrous peridotites to 6.5 GPa and their consequences on the dynamics of subduction zones: Journal of Petrology, v. 46, p. 555–578.

Fumagalli, P., and Stixrude, L., 2007, The 10 angstrom phase at high pressure by first principles calculations and implications for the petrology of subduction zones: Earth and Planetary Science Letters, v. 260, p. 212–226.

Gemmi, M., Fischer, J., Merlini, M., Poli, S., Fumagalli, P., Mugnaioli, E., and Kolb, U., 2011, A new hydrous Al-bearing

pyroxene as a water carrier in subduction zones: Earth and Planetary Science Letters, v. 310, p. 422–428.

Gerya, T.V., Connolly, J.A.D., Yuen, D.A., Gorczyk, W., and Capel, A.M., 2006, Seismic implication of mantle wedge plumes: Physics of Earth and Planetary Interiors, v. 156, p. 59–74.

Griffiths, R.W., and Campbell, I.H., 1990, Stirring and structure in mantle starting plumes: Earth and Planetary Science Letters, v. 99, p. 66–78.

Hirschmann, M.M., 2000, Mantle solidus. Experimental constraints and the effect of peridotite composition: Geochemistry, Geophysics, Geosystems, v. 24, 2000GC000070.

Hirschmann, M.M., Aubaud, C., and Withers, A.C., 2005, Storage capacity of H_2O in nominally anhydrous minerals in the upper mantle: Earth and Planetary Science Letters, v. 236, p. 167–181.

Hosoya, T., Kubo, T., Ohtani, E., Sano, A., and Funakoshi, K.-I., 2005, Water controls the fields of metastable olivine in cold subducting slabs: Geophysical Research Letters, v. 32, L17305.

Ivandic, M., Grevemeyer, I., Bialas, J., and Petersen, C.J., 2010, Serpentinization in the trench-outer rise region offshore of Nicaragua: Constraints from seismic refraction and wide-angle data: Geophysical Journal International, v. 180, p. 1253–1264.

Ivanov, A.V., 2007, Evaluation of different models for the origin of the Siberian Traps, *in* Foulger, G.R., and Jurdy, D.M., eds., Plates, plumes and planetary processes: Geological Society of America Special Paper 430, p. 669–691.

Ivanov, A.V., and Balyshev, S.V., 2005, Mass flux across the lower-upper mantle boundary: Vigorous, absent, or limited? *in* Foulger, G.R., Natland, J.H., Presnall, D.C., and Anderson, D.L., eds., Plates, plumes and paradigms: Geological Society of America Special Paper 388, p. 327–346.

Ivanov, A.V., Demonterova, E.I., Rasskazov, S.V., and Yasnygina, T.A., 2008a, Low-Ti melts from the Southeastern Siberian Traps large igneous province: Evidence for a water-rich mantle source? Journal of Earth System Science, v. 117, p. 1–21.

Ivanov, A.V., He, H., Liekun, Y., Nikolaeva, I.N., and Palesskii, S.V., 2009, $^{40}Ar/^{39}Ar$ dating of intrusive magmatism in the Angara-Taseevskaya syncline and its implication for duration of magmatism of the Siberian Traps: Journal of Asian Earth Sciences, v. 35, p. 1–12.

Ivanov, A.V., He, H., Yan, L., Ryabov, V.V., Shevko, A.Y., Palesskii, S.V., and Nikolaeva, I.V., 2013, Siberian Traps large igneous province: Evidence for two flood basalt pulses around the Permo-Triassic boundary and in the Middle Triassic, and contemporaneous granitic magmatism: Earth-Science Reviews, v. 122, p. 58–76.

Ivanov, A.V., Palesskii, S.V., Demonterova, E.I., Nikolaeva, I.V., Ashchepkov, I.V., and Rasskazov, S.V., 2008b, Platinum-group elements and rhenium in mantle xenoliths from the East Sayan volcanic field (Siberia, Russia): Evaluation of melt extraction and refertilization processes in lithospheric mantle of the Tuva-Mongolian massif: Terra Nova, v. 20, p. 504–511.

Ivanov, A.V., Perepelov, A.B., Palesskii, S.V., and Nikolaeva, I.V., 2008c, First data on the distribution of platinum group elements (Ir, Os, Ru, Pt, and Pd) and Re in island arc basalts of Kamchatka: Doklady Earth Sciences, v. 420, p. 597–601.

Jamais, M., Lassiter, J.C., and Brugmann G., 2008, PGE and Os-isotopic variations in lavas from Kohala Volcano, Hawaii: Constraints on PGE behavior and melt/crust interaction: Chemical Geology, v. 250, p. 16–28.

Kamo, S.L., Czamanske, G.K., Amelin, Yu., Fedorenko, V.A., Davis, D.W., and Trofimov, V.R., 2003, Rapid eruption of Siberian flood-volcanic rocks and evidence for coincidence with the Permian-Triassic boundary and mass extinction at 251 Ma: Earth and Planetary Science Letters, v. 214, p. 75–91.

Khisina, N., and Wirth, R., 2008, Nanoinclusions of high-pressure hydrous silicate, $Mg_3Si_4O_{10}(OH)_2 \cdot nH_2O$ (10Å-phase), in mantle olivine: Mechanisms of formation and transformation: Geochemistry International, v. 46, p. 319–327.

Khisina, N., Wirth, R., Matsyuk, S., and Koch-Muller, M., 2008, Microstructures and OH-bearing nano-iclusions in 'wet' olivine xenocrysts from the Udachnaya kimberlite: European Journal of Mineralogy, v. 20, p. 1067–1078.

Kirby, S.H., Stein, S., Okal, E.A., and Rubie, D.C., 1996, Metastable mantle phase transformations and deep earthquakes in subducting oceanic lithosphere: Reviews of Geophysics, v. 34, p. 261–306.

Komabayashi, T., 2006, Phase relations of hydrous peridotite: implications for water circulation in the Earth's mantle, *in* Jacobsen, S.D., and Van der Lee, S., eds., Earth's deep water cycle: Geophysical Monograph 168, p. 29–43.

Leng, W., and Zhong, S., 2010, Surface subsidence caused by mantle plumes and volcanic loading in large igneous provinces: Earth and Planetary Science Letters, v. 291, p. 207–214.

Lin, J.F., Schwegler, E., and Yoo, C.-S., 2006, Phase diagram and physical properties of H_2O at high pressures and temperatures: Applications to planetary interiors, *in* Jacobsen, S.D., and Van der Lee, S., eds., Earth's deep water cycle: Geophysical Monograph 168, p. 159–170.

Litasov, K., and Ohtani, E., 2003, Stability of various hydrous phases in CMAS pyrolite-H_2O system up to 25 GPa: Physics and Chemistry of Minerals, v. 30, p. 147–156.

Litasov, K.D., 2011, Physicochemical conditions for melting in the Earth's mantle containing a C-O-H fluid (from experimental data): Russian Geology and Geophysics, v. 52 p. 475–492.

Litasov, K.D., and Ohtani, E., 2007, Effect of water on the phase relations in Earth's mantle and deep water cycle, *in* Ohtani, E., ed., Advances in high-pressure mineralogy: Geological Society of America Special Paper, p. 115–156.

Litasov, K.D., Ohtani, E., Kagi, H., Jacobsen, S.B., and Ghosh, S., 2007, Temperature dependence and mechanism of hydrogen incorporation in olivine at 12.5–14.0 GPa: Geophysical Research Letters, v. 34, L16314.

Litasov, K.D., Shatskiy, A., Ohtani, E., and Yaxley, G.M., 2013, Solidus of alkaline carbonatite in the deep mantle: Geology, v. 41, p. 79–82.

Liu, W., and Fei, P.X., 2006, Methane-rich fluid inclusions from ophiolitic dunite and post-collisional mafic-ultramafic intrusions: The mantle dynamics underneath the Paleo-Asian Ocean through to the post-collisional period: Earth and Planetary Science Letters, v. 242, p. 286–301.

McCulloch, M.T., and Gamble, J.A., 1991, Geochemical and geodynamical constraints on subduction zone magmatism: Earth and Planetary Science Letters, v. 102, p. 358–374.

Negredo, A.M., Valera, J.L., and Carminati, E., 2004, TEMSPOL: A MATLAB thermal model for deep subduction zones including major phase transformations: Computers and Geosciences, v. 30, p. 249–258.

Nikishin, A.M., Ziegler, P.A., Abbott, D., Brunet, M.-F., and Cloetingh, S., 2002, Permo-Triassic intraplate magmatism and rifting in Eurasia: implications for mantle plumes and mantle dynamics: Tectonophysics, v. 351, p. 3–39.

Ohtani, E., 2005, Water in the mantle: Elements, v. 1, p. 25–30.
Ohtani, E., and Litasov, K.D., 2006, The effect of water on mantle phase transitions: Reviews in Mineralogy and Geochemistry, v. 62, p. 397–419.
Panina, L.I., and Motorina, I.V., 2013, Meimechites, porphyritic alkaline picrites, and melanephelinites of Siberia: conditions of crystallization, parental magmas, and sources: Geochemistry International, v. 51, p. 109–128.
Pasyanos, M.E., 2010, Lithospheric thickness modeled from long period surface wave dispersion: Tectonophysics, v. 481, p. 38–50.
Pavlenkova, G.A., and Pavlenkova, N.I., 2006, Upper mantle structure of the Northern Eurasia from peaceful nuclear explosion data: Tectonophysics, v. 416, p. 33–52.
Peacock, S.M., 1990. Fluid processes in subduction zone: Science, v. 248, p. 329–337.
Portnyagin, M., Hoernle, K., Plechov, P., Mironov, N., and Khubunaya, S., 2007, Constraints on mantle melting and composition and nature of slab components in volcanic arcs from volatiles (H_2O, S, Cl, F) and trace elements in melt inclusions from the Kamchatka Arc: Earth and Planetary Science Letters, v. 255, p. 53–69.
Priestley, K., and McKenzie, D., 2006, The thermal structure of the lithosphere from shear wave velocities: Earth and Planetary Science Letters, v. 244, p. 285–301.
Puffer, J.H., 2001, Contrasting high filed strength element content of continental flood basalts from plume versus reactivated-arc sources: Geology, v. 29, p. 675–678.
Renne, P.R., and Basu, A.R., 1991, Rapid eruption of the Siberian Traps flood basalts at the Permo-Triassic boundary: Science, v. 253, p. 176–179.
Ryabchikov, I.D., Ntaflos, Th., Büchl, A., and Solovova, I.P., 2001, Subalkaline picrobasalts and plateau basalts from Putorana Plateau (Siberian CFB province). 1. Mineral compositions and geochemistry of major and trace elements: Geokhimiya, v. 5, p. 467–483.
Sakamaki, T., Suzuki, A., and Ohtani, E., 2006, Stability of hydrous melt at the base of the Earth's upper mantle: Nature, v. 439, p. 192–194.
Saito, H., and Suzuki, N., 2007, Terrestrial organic matter controlling gas hydrate formation in the Nankai Trough accretionary prism, offshore Shikoku, Japan: Journal of Geochemical Exploration, v. 95, p. 88–100.
Skiba, S.S., Larionov, E.G., Manakov, A.Y., Kolesov, B.A., and Kosyakov, V.I., 2007, Investigation of hydrate formation in the system H_2-CH_4-H_2O at a pressure up to 250 MPa: Journal of Physical Chemistry B, v. 111, p. 11214–11220.
Sleep, N.H., Meibom, A., Fridriksson, T., Coleman, R.G. and Bird, D.K., 2004, H_2-fluids from serpentinization: geochemical and biotic implications: Proceedings of National Academy of Sciences, v. 101, p. 12818–12823.
Smyth, J.R., Frost, D.J., Nestola, F., Holl, C.M., and Bromiley, G., 2006, Olivine hydration in the deep upper mantle: Effect of temperature and silica activity: Geophysical Research Letters, v. 33, L15301.
Sobolev, A.V., Hofmann, A.W., Kuzmin, D.V., Yaxley, G.M., Arndt, N.T., Chung, S.-L., Danyushevsky, L.V., Elliot, T., Frey, F.A., Garcia, M.O., Gurenko, A.A., Kamenetsky, V.S., Kerr, A.C., Krivolutskaya, N.A., Matvienkov, V.V., Nikogosian, I.K., Rocholl, A., Sigurdsson, I.A., Sushchevskaya, N.M., and Teklay, M., 2007, The amount of recycled crust in sources of mantle-derived melts: Science, v. 316, p. 412–417.
Sobolev, A.V., Krivolutskaya, N.A., and Kuzmin, D.V., 2009a, Petrology of the parental melts and mantle sources of Siberian Trap magmatism: Petrology, v. 17, p. 253–286.
Sobolev, A.V., Sobolev, S.V., Kuzmin, D.V., Malitch, K.N., and Petrunin, A.G., 2009b, Siberian meimechites: origin and relation to flood basalts and kimberlites: Russian Geology and Geophysics, v. 50, p. 999–1033.
Sobolev, S.V., Sobolev, A.V., Kuzmin, D.V., Krivolutskaya, N.A., Petrunin, A.G., Arndt, N.T., Radko, V.A., and Vasiliev, Y.R., 2011, Linking mantle plumes, large igneous provinces and environmental catastrophes: Nature, v. 477, p. 312–316.
Stein, C.A., and Stein, S., 1992, A model for the global variation in oceanic depth and heat flow with lithospheric age: Nature, v. 359, p. 123–129.
Steiner, M.B., 2006, The magnetic polarity time scale across the Permian-Triassic boundary, *in* Lucas, S.G., Cassinis, G., Schneider, G., and Schneider, J.W., eds., Non-Marine Permian biostratigraphy and biochronology: Geological Society London Special Publication 265, p. 15–38.
Sun, S.S., and McDonough, W.F., 1988, Chemical and isotopic systematics of oceanic basalts: Implications for mantle composition and process, *in* Sounders, A.D., and Norry, M.J., eds., Magmatism in the oceanic basins: Geological Society London Special Publication 42, p. 313–345.
Syracuse, E.M., van Keken, P.E., Abers, G.A., 2010, The global range of subduction zone thermal models. Physics of the Earth and Planetary Interiors, v. 183, p. 73–90.
Toksoèz, M.N., Sleep, N.H., and Smith, A.T., 1973, Evolution of the downgoing lithosphere and the mechanisms of deep focus earthquakes: Geophysical Journal of Royal Astronomical Society, v. 35, p. 285–310.
Turcotte, D.L., and Schubert, G., 2002, Geodynamics (second edition): Cambridge, Cambridge University Press, p. 456.
Van der Voo, R., Spakman, W., and Bijwaard, H., 1999, Mesozoic subducted slabs under Siberia: Nature, v. 397, p. 246–249.
Van Keken, P.E., Kiefer, B., and Peacock, S.M., 2002, High-resolution models of subduction zones: Implications for mineral dehydration reactions and the transport of water into the deep mantle: Geochemistry, Geophysics, Geosystems, v. 3, p. 1056.
Vos, W.L., Finger, L.W., Hemley R.J., and Mao, H.-K., 1993, Novel H_2–H_2O clathrates at high pressures: Physical Review Letters, v. 71, p. 3150–3153.
Wang, J., Kalinichev, A.G., and Kirkpatrick, R.J., 2004, Molecular modeling of the 10-Å phase at subduction zone conditions: Earth and Planetary Science Letters, v. 222, p. 517–527.
Wang, J., Kalinichev, A.G., and Kirkpatrick, R.J., 2005, Structure and decompression melting of a novel, high-pressure nanoconfined 2-D ice: Journal of Physical Chemistry B, v. 109, p. 14308–14313.
Williams, Q., and Hemley, R.J., 2001, Hydrogen in the deep Earth: Annual Review of Earth and Planetary Sciences, v. 29, p. 365–418.
Wirth, R., Vollmer, C., Brenker, F., Matsyuk, S., and Kaminsky, F., 2007, Inclusions of nanocrystalline hydrous aluminium silicate 'Phase Egg' in suprdeep diamonds from Juina (Mato Grosso State, Brazil): Earth and Planetary Science Letters, v. 259, p. 384–399.
Wooden, J.L., Czamanske, G.K., Fedorenko, V.A., Arndt, N.T., Chauvel, C., Bouse, R.M., King, B.-S.W., Knight, R.J., and Siems, D.F., 1993, Isotopic and trace-element constraints on mantle and crustal contributions to characterization of Siberian continental flood basalts, Noril'sk area, Siberia: Geochimica et Cosmochimica Acta, v. 57, p. 3677–3704.
Yasuda, A., and Fujii, T., 1998, Ascending subducted oceanic crust entrained within mantle plumes: Geophysical Research Letters, v. 25, p. 1561–1564.

Yarmolyuk, V.V., Litvinovsky, B.A., Kovalenko, V.I., Jahn, B.M., Zanvilevich, A.N., Vorontsov, A.A., Zhuravlev, D.Z., Posokhov, V.F., Kuz'min, D.V., and Sandimirova, G.P., 2001, Formation stages and sources of the peralkaline granitoid magmatism of the Northern Mongolia-Transbaikalia rift belt during the Permian and Triassic: Petrology, v. 9, p. 302–328.

Zorin, Y.A., 1999, Geodynamics of the western part of the Mongolia-Okhotsk collisional belt, Trans-Baikal region (Russia) and Mongolia: Tectonophysics, v. 306, p. 33–56.

Zorin, Yu.A., Turutanov, E.Kh., Kozhevnikov, V.M., Rasskazov, S.V., and Ivanov, A.V., 2006, The nature of Cenozoic upper mantle plumes in East Siberia (Russia) and Central Mongolia: Russian Geology and Geophysics, v. 47, p. 1046–1059.

Zorin, Yu.A., and Vladimirov, B.M., 1989, On the genesis of trap magmatism of the Siberian platform: Earth and Planetary Science Letters, v. 93, p. 109–112.